npj | clean water

www.nature.com/npjcleanwater

ARTICLE OPEN

Denitrification mechanism in oxygen-rich aquatic environments through long-distance electron transfer

Ming-Zhi Wei[1,6], Jin-Wei Liu[1,6], Qin-Zheng Yang[2], An Xue[1], Hao Wu[3], Jin-Ren Ni[1], Lea R. Winter[4], Menachem Elimelech[4]✉ and Hua-Zhang Zhao[1,5]✉

The lack of electron donors in oxygen-rich aquatic environments limits the ability of natural denitrification to remove excess nitrate, leading to eutrophication of aquatic ecosystems. Herein, we demonstrate that electron-rich substances in river or lake sediments could participate in long-distance electron rebalancing to reduce nitrate in the overlying water. A microstructure containing *Dechloromonas* and consisting of an inner layer of green rust and an outer layer of lepidocrocite forms in the sediment-water system through synergetic evolution and self-assembly. The microstructure enables long-distance electron transfer from the sediment to dilute nitrate in the overlying water. Specifically, the inner green rust adsorbs nitrate and reduces the kinetic barrier for denitrification via an Fe(II)/Fe(III) redox mediator. Our study reveals the mechanism of spontaneous electron transfer between distant and dilute electron donors and acceptors to achieve denitrification in electron-deficient aquatic systems.

npj Clean Water (2022)5:61 ; https://doi.org/10.1038/s41545-022-00205-x

INTRODUCTION

As a relatively stable nitrogen species, nitrate can persistently reside in the overlying water of aquatic ecosystems[1,2]. Excessive nitrate causes algal blooms, increases water treatment costs, and endangers human health[3]. At present, over 63% of the world large inland lakes suffer from eutrophication caused by high concentrations of nitrate[4]. Hence, reducing nitrate concentration is of great significance for enhancing the ecological and socio-economic values of aquatic systems.

Nitrate can be reduced by the assimilation of aquatic plants and phytoplankton in natural water environments[5,6]. In addition, nitrate is mainly removed through dissimilation by denitrification, where electron donors in anoxic environments (e.g., organic matter and sulfide) reduce nitrate to nitrogen gas through a complex pathway involving microorganisms[7,8]. In the overlying water of aquatic environments, however, there is a relatively high concentration of dissolved oxygen (2−6 mg/L)[9]. Previous studies suggested that dissolved oxygen concentration above 0.5 mg/L would inhibit denitrification[10,11] because oxygen and nitrate are in a fierce competition for electrons. As a result, electron donors in the overlying water would be largely oxidized and consumed by aerobic bacteria instead of effectively be used for denitrification. It is generally accepted that there are not sufficient electron donors and anaerobic/anoxic environments required for denitrification, resulting in nitrate existing stubbornly in the overlying water of aquatic ecosystems.

Sediments in aquatic systems, however, contain large amounts of sulfide, organic matter, and other reducing substances. For example, it was reported that the average loss on ignition of sediments in lakes in Iowa is 10.3%[12], and the acid volatile sulfide in the river sediments in Shanghai is 5 mmol/kg[13], indicating that sediments can provide abundant electrons[14–17]. Considering nitrate and other electron-deficient substances in the overlying water of aquatic ecosystems, an electron imbalance caused by this electron spatial separation widely exists in natural water environments. Herein, we pose the question: Can these electrons in sediments be transferred to overlying water and used for denitrification to achieve electron rebalance? Several studies have reported that cable bacteria in the suboxic zone of the sediment surface can achieve electron transfer over a distance of 1–2 cm[18,19]. However, there is a much greater distance for electrons to transport from the sediment to the overlying water for nitrate reduction. The problem is further complicated by the competition between nitrate and oxygen in the overlying water for harvesting these electrons. To date, there are no studies demonstrating how nature can overcome these two challenging problems to achieve denitrification in overlying water of aquatic environments.

Electrons can be transported by microorganisms mediated by substances such as conductive minerals and electron carriers[20,21] Past studies demonstrated that it is feasible for microorganisms to donate electrons to these conductors or semiconductors and obtain electrons from them, as long as the interfacial barrier between the microorganisms and these conductors/semiconductors be overcome[22,23]. Bacteria can use α-Fe_2O_3, Fe_3O_4, MnO_2, and other conductors or semiconductors to transfer electrons[24–26]. Driven by the potential difference between the overlying water and the sediment (generally about 0.7 V)[27], the electrons in the sediment theoretically tend to transfer upward to accomplish electron rebalance. Relying on the extension of these conductors/semiconductors into the aqueous solution, it may be possible for electrons in sediments to be transported over long distance, but the feasibility of this process needs to be verified. However, if this process is feasible, the electrons transferred to the overlying water are more likely to be captured and utilized by oxygen under typical conditions with relatively high concentration of dissolved oxygen and low concentration of nitrate. Can Nature create a

[1]Key Laboratory of Water and Sediment Sciences (Ministry of Education), College of Environmental Sciences and Engineering, Peking University, Beijing 100871, China. [2]State Key Laboratory of Biobased Material and Green Papermaking, Qilu University of Technology, Shandong Academy of Sciences, Jinan 250353, China. [3]Hebei Key Laboratory of Heavy Metal Deep-Remediation in Water and Resource Reuse, Yanshan University, Qinhuangdao 066004, China. [4]Department of Chemical and Environmental Engineering, Yale University, New Haven, CT 06520-8286, USA. [5]Shanxi Laboratory for Yellow River, College of Environmental and Resource Sciences, Shanxi University, Taiyuan 030006, China. [6]These authors contributed equally: Ming-Zhi Wei, Jin-Wei Liu. ✉email: menachem.elimelech@yale.edu; zhaohuazhang@pku.edu.cn

special environment for electrons to be selectively transferred to nitrate? This question is beyond our imagination.

In this study, we reveal that electrons can be transferred from sediments to the overlying water for denitrification, realizing electron rebalance in water environments. We have shown that in the water-sediment system, iron oxide and bacteria dynamically co-evolve to form a two-layer three-dimensional microstructure, which can overcome the physical limitation and realize long-distance electron transfer. The unique green rust in the microstructure can adsorb nitrate from water through ion exchange and locally enrich its concentration, thus improving the competitiveness of nitrate against oxygen and realizing selective reduction of nitrate with sediment electrons. We further elucidate the formation mechanism of the new denitrification pathway, which has important implications for water pollution remediation and the nitrogen geochemical cycle.

RESULTS

Formation of self-assembled microstructure

The simulated Fe-sediment system included an iron rod with one end placed in the sediment and the other end exposed to a low concentration of nitrate in the overlying water (Fig. 1a). After the introduction of the iron rod to the system, its smooth surface developed a loose coating. The coating consisted of two layers which were visible to the naked eye: (i) a dark brown and relatively fluffy outer layer and (ii) a dark green inner layer closely attached to the surface of the iron rod. Using scanning electron microscopy, we observed that the outer iron oxide crystals were needle-shaped, while the inner crystals were mainly regular hexagons, with bacteria attached to them (Fig. 1b). These results demonstrate that the microstructure is markedly different from traditionally perceived biofilms and does not consist of a single type of iron oxide. Rather, this microstructure is an electron mediator that differs from those reported in the literature: it is neither a simple biofilm nor a natural substance added artificially or from the environment. This microstructure spontaneously formed on the surface of the iron rod along with the decrease in nitrate concentration. Copper rod (Cu-sediment system) and stainless-steel rod (SS-sediment system) were used for comparison to investigate if long-distance electron transfer can be accomplished by other metal rods. These systems showed almost no change of the rod surface compared to the pristine surface, with no microorganisms attached and no structure formed (Supplementary Fig. 1).

Nitrate reduction efficiency can indicate the electron transfer efficiency of the system. After the iron rod was introduced into the sediment-water system, it passed a four-day adaptation period before nitrate reduction was observed. Within the next 12 days, the concentration of nitrate in the overlying water was rapidly reduced from 2.1 mg-N/L to 0.3 mg-N/L, dropping to almost zero by Day 20. During the first cycle of 25 days, the NO_3^- removal efficiency reached 98.6% (Fig. 2a). In contrast, the nitrate reduction in control groups with only sediment, only iron rod, and SS-sediment and Cu-sediment systems (Supplementary Fig. 2) showed some nitrate reduction, but significantly less than the Fe-sediment system. The results with the Fe-sediment, only sediment, and only iron rod systems indicate that the electrons for nitrate reduction in the Fe-sediment system were neither from the sediment by diffusion nor from the iron rod by self-corrosion. Further, comparing the results with the Fe-sediment, SS-sediment, and Cu-sediment systems indicate that the long-distance electron transfer could not be accomplished only by electron conduction, but rather strongly relying on the microstructure formed on iron rod. At the same time, NH_4^+-N and NO_2^--N did not increase along with the decrease of nitrate concentration in the control groups, which suggests that there was no direct nitrate reduction to ammonium and nitrite. By assessing the stability over three 25-day cycles, we found that the Fe-sediment system maintained outstanding degradation activity during the second and third cycles. In fact, the spontaneously-formed double-layer, three-dimensional microstructure reduced the adaption time of the Fe-sediment system to three days and one day for the second and third cycles, respectively, suggesting that the microstructure improved the electron transfer from sediment to nitrate.

We tested the electron transfer performance of the iron rod by cyclic voltammetry (CV) and electrochemical impedance spectroscopy (EIS). A strong oxidation peak was observed from −0.25 V to 0.25 V and a reduction peak appeared between −0.75 V and −0.25 V on Day 25, which suggested that the structure formed on

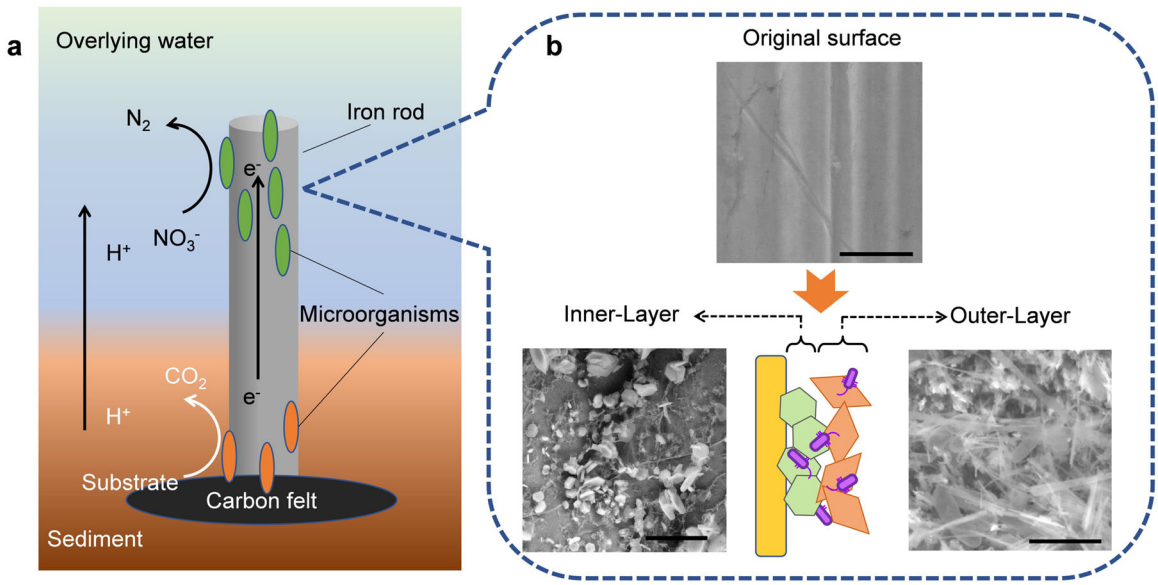

Fig. 1 Nitrate reduction process of Fe-sediment system and changes of iron rod surface. a Nitrate reduction process induced by iron rod. Electrons in sediment are conducted by an iron rod and transferred to nitrate in the overlying water. **b** SEM images of iron rod surface changes. The surface of the iron rod changed from the initial smooth state to a double-layer structure. The outer-layer crystals were needle-shaped, while the inner-layer crystals were mainly regular hexagons. Scale bars, 2 μm.

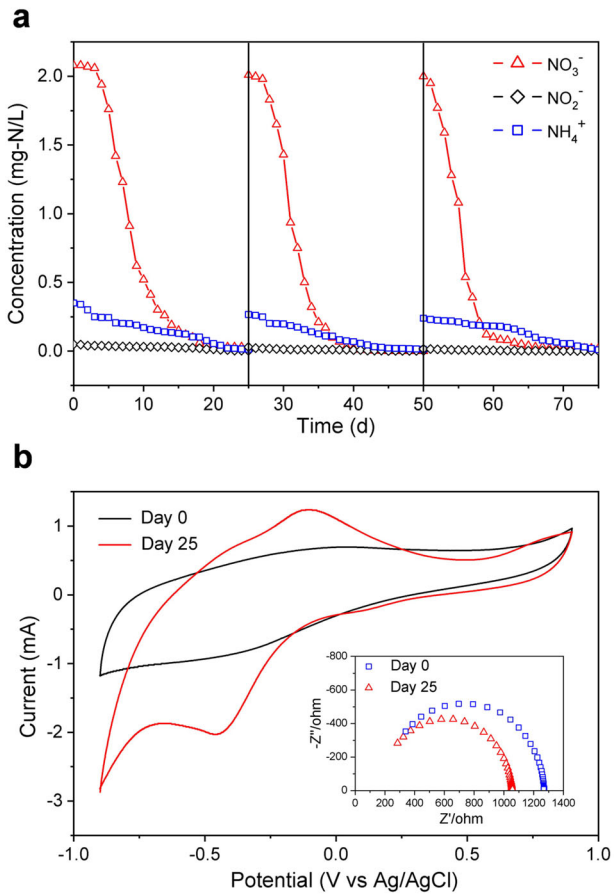

Fig. 2 NO_3^- removal and electron transfer efficiency in Fe-sediment system. a NO_3^- removal efficiency of Fe-sediment system over 3 cycles of 25 days each. The overlying water initially contained 2.1 mg-N/L NO_3^- (pH 7.6, 25°C). **b** Cyclic voltammetry curves at a scan rate of 0.1 mV/s, and Nyquist plots (inset) in the frequency range of 100 kHz to 0.1 Hz in 2.1 mg/L NO_3^--N solution before the rod was introduced and after one cycle with the iron rod.

the iron rod surface could be used as an electron mediator for redox reactions[28]. Moreover, the shape of the voltammogram was typical for bacteria, whose electrochemical activity is ascribed to outer membrane cytochromes[29]. The increased peak current intensity with respect to the pristine iron rod indicated improvement of electron transfer performance[30] (Fig. 2b). EIS analysis showed that the internal charge transfer resistance was significantly reduced from 1267 Ω on Day 0 to 1057 Ω on Day 25, which suggested that the formation of microstructures substantially increased the bioelectrochemical extracellular electron transfer rate[31] (Fig. 2b, inset).

In summary, the high nitrate reduction activity and electron transfer performance suggest that the three-dimensional structure improves the electron transfer efficiency between the iron rod and NO_3^- on the microscale. On the system level, the Fe-sediment system enables effective nitrate reduction, concomitantly completing the electron rebalancing process between electrons from sediment and NO_3^- in the overlying water.

Iron oxides in the microstructure

The iron oxides formed on the surface of the iron rod after one 25-day cycle were determined using Mössbauer spectroscopy to be Fe(III) and Fe(II)/Fe(III) (Fig. 3a). Based on the XRD pattern, the main component of the iron oxides in the inner layer of the rod surface was green rust ($GR(CO_3^{2-})$) (Fig. 3b), where strong absorption peaks of $GR(CO_3^{2-})$ can be seen at $2\theta = 11.80°$ and 23.69°. The iron oxides on the outer layer of the iron rod surface appeared at $2\theta = 14.20°$, 27.12°, 36.36°, 38.14°, 46.92°, 52.84°, and 60.78°. These characteristic XRD peaks showed that the iron oxide on the iron rod surface was mainly lepidocrocite (γ-FeOOH). As a result, a self-assembled double-layer iron oxides structure with an inner layer of green rust and an outer layer of lepidocrocite formed on the iron rod.

To evaluate the electron transfer and nitrate reduction efficiency of the double-layer iron structure compared to other iron oxide compositions and structures, we replaced the iron rod with two other types of iron oxide rods. One was an air-calcined iron rod (FeOA-sediment system) with iron oxide composed of magnetite, hematite, and goethite; and the other was an iron rod soaked in water (FeOW-sediment system) mainly composed of lepidocrocite (Supplementary Fig. 3). These two iron oxide rod systems had lower nitrate removal efficiencies than the Fe-sediment system, and the nitrate removal rates were gradual in contrast to the rapid reaction period observed for the Fe-sediment system on Days 4–16 (Supplementary Fig. 5). Both results suggest that the two iron oxide rod systems could not achieve high nitrate reduction performance because the iron rod surfaces did not form the double-layer green rust-lepidocrocite structure. In all, these results indicate that only the self-assembled double-layer, three-dimensional network structure composed of bacteria and inner-green rust-outer-lepidocrocite can achieve efficient electron transfer and nitrate reduction, whereas systems consisting only of iron oxides formed on the surface of the iron rod are significantly less efficient.

Green rust is a layered double hydroxide with mixed valence states of Fe(II)/Fe(III); the valence state conversion of Fe(II) and Fe(III) can be realized within the green rust crystals[32]. Electrons were transferred from the sediment through the iron rod to microorganisms for nitrate reduction, which enabled green rust on the inner surface of the rod to accept electrons. Green rust can co-exist with many kinds of microorganisms[33]. In the network structure formed on the iron rod, the corrosion caused by microorganisms on the green rust crystals (Fig. 3c) and microbial attachment within the green rust crystals can be observed through SEM (Supplementary Fig. 4). As a layered double hydroxide, green rust is a potential adsorbent[34], and the anions in its layers can be exchanged with nitrate ions in water. Through elemental composition analysis, we found that the main elements of the green rust are C, O, Fe, and N (Fig. 3c), which further verified that the green rust is $GR(CO_3^{2-})$. The detection of N is consistent with the adsorption of nitrate by the green rust. Therefore, the nitrate in the surrounding water may be enriched near the microstructure, thereby promoting the accumulation of denitrifying bacteria and enhancing electron transfer to nitrate over other electron acceptors despite the low bulk nitrate concentration (Fig. 2a).

Microbial community and gene composition in the microstructure

By analyzing the microbial community on the iron rod through high-throughput sequencing, we found that autotrophic denitrifying bacteria (~43.4%) accounted for the largest proportion of the microstructure (Fig. 4a), including *Dechloromonas* (28.5%), *Simplicispira* (11.6%), *Hydrogenophaga* (2.0%) and *Sulfuricurvum* (1.3%). In addition, iron redox bacteria such as *Dechloromonas* and *Sediminibacterium* (3.3%), also occupied a considerable proportion of the community. As a result, we can infer that the iron rod microstructure hosted an autotrophic microbial community that efficiently coupled with iron redox electrochemistry to accomplish nitrate reduction.

We analyzed the KEGG gene through functional annotation and hierarchical classification, detecting a total of 11,108,018 functional gene read frames. *Dechloromonas* contributed 34.3% and

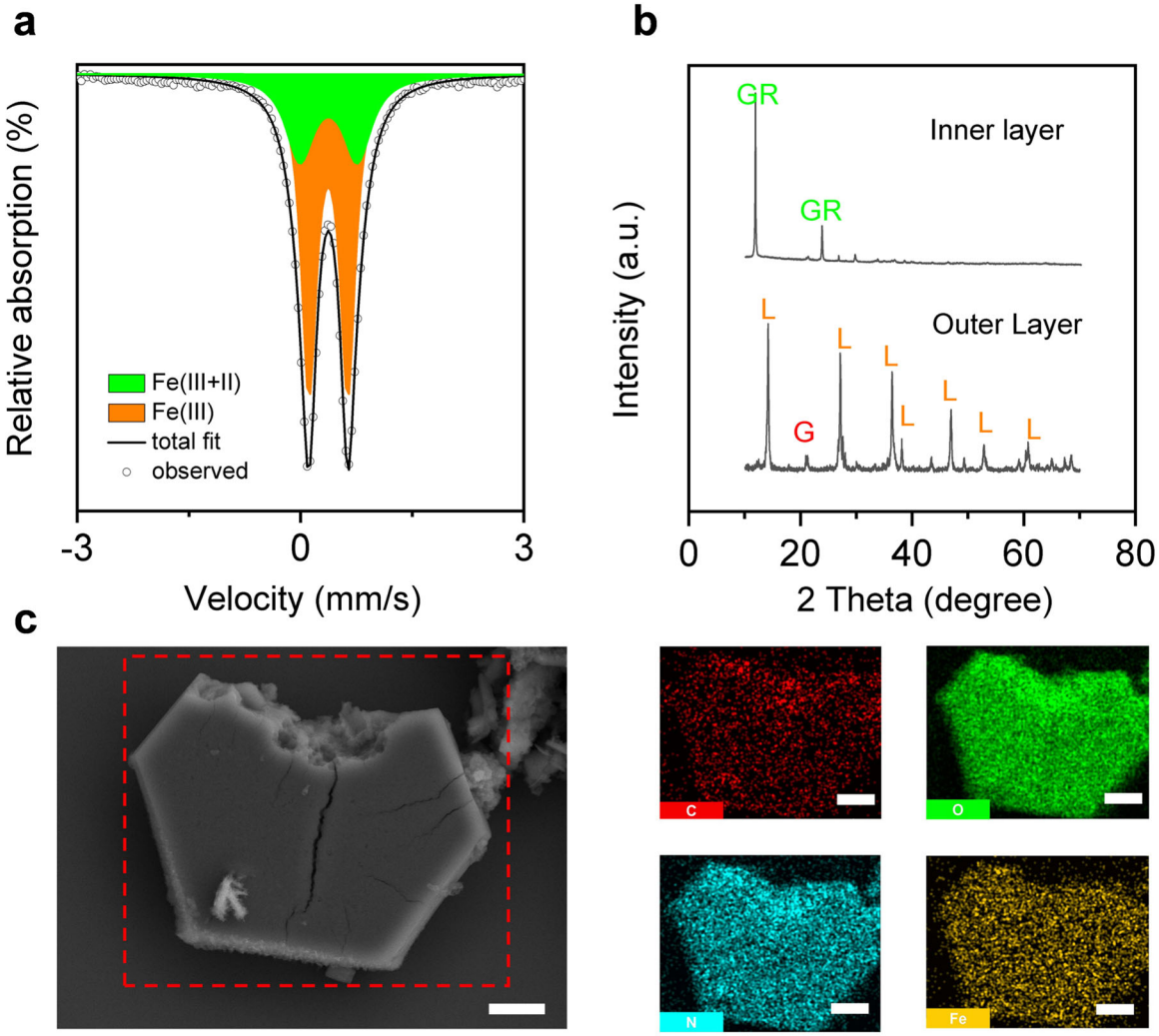

Fig. 3 Iron oxidation state identification in the microstructure on iron rod in Fe-sediment system. a Mössbauer spectrum of surface iron oxides on the iron rod measured at room temperature (293 K) and fitted with the hopping relaxation model. Fe(III) (orange, 66.5%) and Fe(III)/Fe(II) (green, 33.5%) doublets are shown, and the sum of modeled components are shown as the solid black line. **b** X-ray diffraction patterns of iron oxide inner and outer layers. (G-goethite, L-lepidocrocite and GR-green rust). **c** Scanning electron microscope images and energy dispersive X-ray spectroscopy analysis of microbial corrosion on a green rust crystal. (C, red; O, green; N, blue; Fe, yellow). Scale bars, 2 μm.

94.1% of the reading frame of the CO_2 fixation genes *IDH1* and *NIFJ*, respectively, and accounted for 44.6% of the total CO_2 fixed gene reading frame of the iron rod bacterial consortium (Supplementary Table 1 and Supplementary Fig. 6). This suggests that *Dechloromonas* functioned as an autotrophic strain. The KEGG gene analysis resulted in 88,540 denitrification metabolism-related reading frames (Supplementary Table 2). The strains of *Dechloromonas* genus accounted for 88.2% of *napA* (periplasmic nitrate reductase), 79.7% of *norB* (nitric oxide reductase), and 65.4% of *nosZ* (nitrous-oxide reductase) (Fig. 4b), indicating that the primary bacteria involved in denitrification were *Dechloromonas* strains, which likely enabled *Dechloromonas* to predominate due to the abundance of nitrate. Although *Dechloromonas* did not contain the gene *nirK* which can convert NO_2^- to NO and N_2O, another dominant strain, *Methylotenera*, accounted for 90.4% of *nirK* for denitrification. In addition, the *narG* gene (membrane-bound nitrate reductase) in genus *Acidovorax* can promote the reduction of NO_3^--N inside the microbial cell. It can be inferred that the nitrate, nitrite, nitric oxide, and nitrous oxide reductases corresponding to these genes played an important role in NO_3^--N reduction; thus NO_3^--N was finally converted into N_2 through intermediate products such as nitrite, nitric oxide, and nitrous oxide[35]. These results also suggest that the denitrification in the microstructure is accomplished mainly by *Dechloromonas*, along with the synergetic contributions of various bacteria.

Dechloromonas contains a series of functional genes for the complex transportation, exportation, and oxidation/reduction of iron (Supplementary Table 3). These bacteria can also coexist with a variety of iron-containing compounds[36] and use Fe(II) as an electron donor for electron transfer[37]. The abundance of these iron-related genes was very low in other strains of the microbial community (Fig. 4b). Furthermore, *Dechloromonas* contained 53% of c-type cytochrome genes in the microstructure community, where these genes represent 0.45% of the total functional abundance (Supplementary Table 2). The c-type cytochrome can transfer the electrons obtained from the oxidation of the outer membrane of the cell to the quinone pool of the inner membrane to accomplish denitrification[38].

Adaptive dynamic formation process of the microstructure

We found that the microstructure of the iron rod surface was formed through dynamic changes. Through XPS analysis, we found that the O1s peak of the sample taken from the surface on Day 2 was 531.5 eV, and it shifted to 531.3 eV and 531.1 eV on

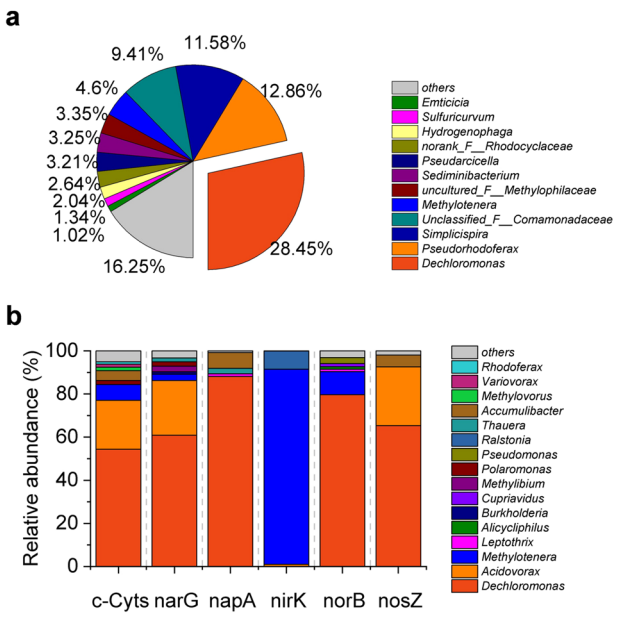

Fig. 4 Functional bacterial community and genes in the microstructure on iron rod in Fe-sediment system. a Bacterial community composition in the microstructure. **b** Distribution of denitrification genes in the iron rod surface microstructure. The category "others" represents the genera and genes with relative abundances below 1%.

Days 9 and 25, respectively (Supplementary Fig. 7). We used XRD to analyze the composition of the iron oxides. The inner layer of iron oxides did not form until Day 6 (Fig. 5a). The strong diffraction peaks at 2θ of 11.80°, 23.69° and 33.18°Confirmed that the main component of the iron oxides was GR(CO_3^{2-}), which remained stable through the rest of the cycle. Regarding the outer layer of iron oxides, the strong diffraction peak at 2θ = 20.88° and two weak diffraction peaks at 2θ = 26.68° and 51.42° on Day 2 (Fig. 5b) indicated that the initial flocculated material on the iron rod outer surface was mainly goethite (α-FeOOH). The XRD characteristic peaks on Day 9 and Day 25 appeared at 2θ = 14.20°, 27.12°, 36.36°, 38.14°, 46.92°, 52.84°, and 60.78°, indicating that the iron oxides on the iron rod outer surface had been converted to lepidocrocite (γ-FeOOH) (Fig. 5a). Therefore, the iron oxides generated in situ on the iron rod gradually stratified after the rod was introduced into the sediment-water system, forming a stable structure dominated by an inner layer of green rust and an outer layer that transformed from goethite to lepidocrocite.

Regarding the bacterial consortium, we found that the community was constantly changing, which is consistent with the observation that the iron oxides transformed over time. Through high-throughput sequencing technology, we found that the α diversity index decreased as nitrate reduction progresses (Supplementary Fig. 8). Furthermore, the abundance of bacterial genus with a relative abundance of less than 1% in the microstructure added up to 33.5% on Day 6, and this proportion decreased to about 16% on Day 25. These results suggest that dynamic changes of the community lead to the emergence of dominant strains. At the initial stage (Days 1–9), the main bacterial population on the iron rod surface consisted of the hydro-autotrophic denitrifying bacteria *Hydrogenophaga*[39] (25.5% on Day 6) (Fig. 5b). Some sulfur-oxidizing, nitrate-reducing bacteria such as *Thiobacillus* and *Sulfuricurvum*, with their ability to obtain electrons from the iron rod for nitrate reduction[40], were present; their abundance was relatively high in the early stage (for example, *Thiobacillus* at 3.3% on Day 6 and *Sulfuricurvum* at 8.0% on Day 6). Therefore, the early microbial community was dominated by hydro-autotrophic and sulfur-autotrophic microorganisms.

While electron transport occurred in the system, the formation of iron oxides on the rod surface prevented bacteria such as *Hydrogenophaga* from achieving direct contact with iron, where *Hydrogenophaga* consume hydrogen generated by the direct reaction of iron and water[41]. These bacteria therefore received insufficient electrons and were gradually eliminated by the system. Microorganisms which were adapted to the iron-nitrate environment gradually grew to dominate the microstructure. The nitrate-reducing, iron-oxidizing bacteria *Dechloromonas* grew from an abundance of about 3% on Day 9 to nearly 28.5% on Day 25. In addition, bacteria that rely on iron respiration, such as the iron-reducing bacteria *Rhodobacter* and iron-oxidizing bacteria *Sediminibacterium*[36], gradually appeared in the community. *Rhizobia* that inhibit iron corrosion, such as *Allorhizobium-Neorhizobium-Pararhizobium-Rhizobium*, existed in the bacterial community in low abundance (such as 2.4% on Day 21) throughout the process. After Day 21, the microbial community transformed into a community whose primary function was nitrate reduction.

DISCUSSION

In our system, the upper end of the iron rod was in a nitrate-containing solution with a high redox potential, and the lower end of the rod was inserted into a sediment with a low redox potential. Therefore, an electron imbalance was established between the upper and lower ends of the iron rod. In the first few days, microorganisms gradually attached to the surface of the iron rod. *Hydrogenophaga*, for example, can consume H_2 produced by iron oxidation to accomplish nitrate reduction and promote an early attachment of microorganisms on the rod, which simultaneously accelerated iron corrosion[42]. Due to these microorganisms, a layer of iron oxides dominated by goethite was formed on the surface of the rod, which in turn led to the gradual decrease in abundance of several genera (Fig. 4). Goethite has good biocompatibility and encouraged the growth of denitrifying microorganisms. Since the outer iron oxide layer was in contact with more oxygen, it mainly consisted of Fe(III) oxide; in contrast, the inner layer formed Fe(II)/Fe(III) oxide due to the existence of oxygen-consuming microorganisms and the continuous inflow of electrons to the iron rod surface. Due to the presence of the microorganisms, green rust is formed in the inner iron rod layer. The outer layer of the iron hydroxide lepidocrocite may be formed partially by the conversion of goethite from the early stage. For example, *Acidovorax* can promote the conversion of goethite to lepidocrocite on the iron rod surface[43], and lepidocrocite can be produced by biotic[44] or abiotic[45] transformation of green rust. These dynamic changes result in the stable double-layer structure of inner green rust and outer lepidocrocite. (Fig. 1b, Fig. 3a, b)

Dechloromonas can participate in the iron redox cycle and complete the ferrous oxidation-nitrate reduction process[46]; its abundance gradually increases in the system (Fig. 5b). Green rust –– with its Fe(II)/Fe(III) complex valence state –– has been found to reduce NO_3^--N to NH_4^+-N with or without biological participation[47,48], although the nitrogen remains in the water as NH_4^+-N rather than being removed. In the present synergetic evolutionary and self-assembled system, the contributions of the denitrifying microorganism *Dechloromonas* prevented NO_2^--N and NH_4^+-N accumulation (Fig. 2a). The lack of accumulation of these partial reduction products indicated either that green rust had a weak effect on the abiotic reduction of nitrate or that the abiotic reduction products of green rust were utilized by microorganisms attached to the outer layer to complete the process of reducing NO_3^--N to N_2. The influence of *Dechloromonas* on iron corrosion varies according to its environment. In the electron rebalancing system of the present study, the iron oxide is active green rust and lepidocrocite, rather than the previously

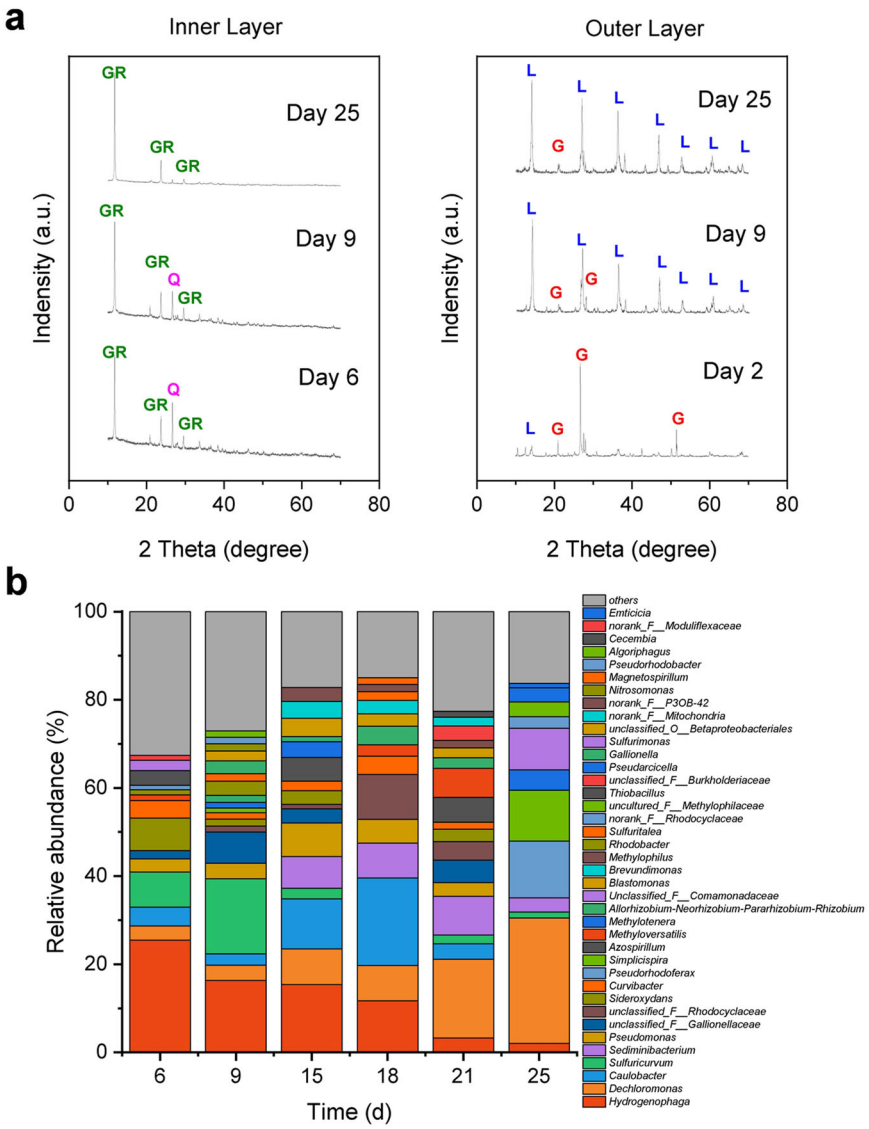

Fig. 5 Transformation of iron oxides and bacterial community in Fe-sediment system. a Dynamic changes of iron oxides composition in the inner layer (left) and outer layer (right) on iron rod surface after the iron rod was introduced into the sediment-water system, revealed by X-ray diffraction patterns. (G-goethite, L-lepidocrocite, GR-green rust and Q-quartz). **b** Evolution of bacterial community on iron rod surface during nitrate reduction. The category "others" represents the genera with relative abundances below 1%.

studied magnetite[49]. Owing to the existence of microorganisms and the continuous inflow of electrons from sediment, the green rust in the microstructure did not transform to magnetite or trivalent goethite[48] and other inert iron oxides. Therefore, the two-layer, three-dimensional network structure formed by the synergetic evolution of iron oxides and microorganisms remained in an active state, simultaneously mediating electron transfer and nitrate reduction.

Thus, we conclude that under electron imbalance conditions, a double-layer, three-dimensional network structure arises from the synergetic evolution and self-assembly of microorganisms and iron oxides. The formation of this microstructure enhances the reduction of the low-concentration nitrate, thereby accomplishing electron rebalance for the system. Electrons generated by the oxidative decomposition of organic matter in sediment are transferred along the iron rod to iron oxides on the surface of the rod, enabling electron transfer to the three-dimensional network. Electrons are transferred from the iron oxides to denitrifying bacteria such as *Dechloromonas* in the radial direction of the iron rod via divalent iron. Finally, the electrons are passed to NO_3^--N through a series of extracellular electron transfers and denitrifying proteins to complete the nitrate reduction. During this process, the green rust iron in the inner layer dynamically changes between divalent and trivalent oxidation states as electrons are transferred between the iron rod and bacteria. We demonstrate that electrons from the sediment are transported to aqueous NO_3^--N through an iron rod microstructure composed of an inner surface layer of green rust, an outer lepidocrocite surface layer, and a *Dechloromonas*-dominated bacterial community (Fig. 6).

In conclusion, we discovered that the formation of a microstructure on the surface of the iron rod involves self-assembly and synergetic evolution. Since iron and bacteria are ubiquitous in nature, by studying the dynamic process occurring on the iron rod in the sediment-water system, we provide an example of how nature can achieve electron rebalancing processes between electron-rich and electron-deficient substances, even if these substances are spatially distanced and at low concentrations. This new way of electron transfer could possibly be seen in nature when there are related iron oxides and bacteria on lake banks or bridge piers. In addition, our research

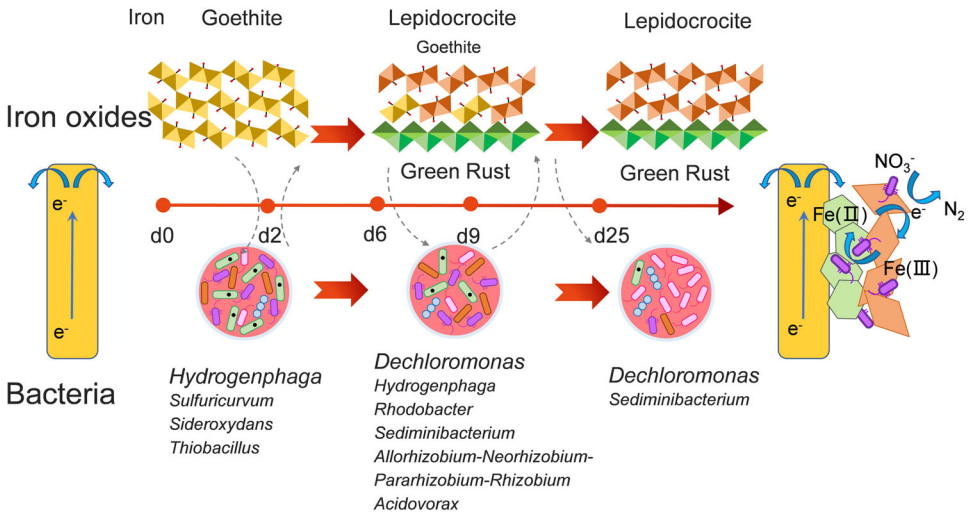

Fig. 6 Timeline of microstructure formation by the synergistic evolution of iron oxides and bacteria. To achieve electron rebalancing of the system, corrosion occurs on the surface of the iron rod, accompanied by the transformation of the bacterial community. Iron oxides and the bacterial community synergistically assemble to form the microstructure, which promotes electron transfer from the surface of the iron rod to nitrate in the overlying water.

has potential application in environmental remediation, including reducing electron-deficient compounds such as nitrate in wastewater and oxidizing electron-rich substances such as organic matter in sediments or soil. Considering the wide abundance of iron and bacteria and the simplicity of this system, this new strategy for environmental remediation would be cost-effective and readily implemented.

METHODS

Preparation of sediment-water systems

A sediment sample (600 mL), freshly collected from Beijing Purple Bamboo Park, was put in a 48 cm-high, 2 L graduated cylinder (I.D. 9.0 cm). A 0.3 cm-thick carbon felt (I.D. 7.0 cm) was positioned at the 300 mL mark of the cylinder in the sediment. Two liters of 2.0 mg/L sodium nitrate solution prepared with municipal tap water were added to the cylinder as the overlying solution, which was exposed to air all the time. A 25.0 cm polished iron rod (I.D. 1.0 cm) was inserted vertically into the sediment with the bottom end tightly in contact with the carbon felt. The top end of the iron rod was 10.0 cm lower than the surface of the water (Fig. 1). This system was kept at room temperature for three 25-day cycles. The sodium nitrate overlying solution was replaced between cycles. The Cu-sediment system, SS-sediment system, FeOW-sediment system and FeOA-sediment system were also prepared as control groups, as described in the SI.

Iron rod characterization

A piece of the iron rod was cut, immersed in 2.5% glutaraldehyde for two hours, carefully rinsed three times with phosphate buffer (50 mM, pH 7.0) for 20 minutes, sequentially dehydrated with 30%, 50%, 70%, 90% and 100% (v/v) ethanol for 15 minutes, freeze-dried, and imaged with a scanning electron microscope (SEM) (Quanta200F, FEI) equipped with an energy dispersive X-ray detector for elemental analysis under low vacuum conditions. The iron oxides on the iron rod surface were collected from the iron rod under anaerobic conditions, freeze-dried, and analyzed using X-ray diffraction (XRD) with a Bruker D8 Discover instrument (Bruker AXS GmbH, Germany) equipped with a D/max-γ B diffractometer and using Cu Kα radiation in the 2θ range from 10.00° to 70.00°. The elemental composition and oxidation states were characterized with X-ray photoelectron spectroscopy (XPS) (Axis Ultra, Kratos Analytical Ltd., Manchester, UK) equipped with a monochromatic Al Kα radiation source (225 W, 15 mA, 15 kV) at the pass energy of 160 eV for wide spectra and 40 eV for individual photoelectron lines. The binding energy (BE) scale was referenced to the C1s line of aliphatic carbon. The spectra were analyzed in the CASAXPS software. For the Mössbauer analysis, the iron oxides sample (100–200 mg) was collected under anoxic water, transferred to an anaerobic glovebox chamber (100% N_2 atmosphere, <0.1 ppm O_2), dried, mixed with Vaseline, placed in a Cu sample tube (I.D. 1.3 cm), and sealed with two pieces of Kapton tape. Mössbauer spectra were recorded on a Topologic 500 A spectrometer coupled with a time-proportional controller using ^{57}Co(Rh) moving in the constant acceleration mode as the γ-ray radioactive source. The velocity was calibrated with a 25 μm α-Fe foil, and the isomer shift (I.S.) was measured from the center of a-Fe at room temperature. The spectrum was fitted with the hopping relaxation model[50].

Microbial community and metagenomic analysis

Two biomass samples were collected in two independent experiments for the amplicon sequencing and metagenomics; we chose one group of data for analysis. The biomass on the upper part of the iron rod was collected, dispersed into a 50 mL sterile tube, centrifuged at 2700 ×g for five minutes at 4 °C, and extracted with the FastDNA® Spin Kit for Soil (MP Biomedicals, LLC, Illkirch, France) according to the manufacturer's instruction. The extracted total genomic DNA was subject to PCR amplification targeting the 16 S rRNA hypervariable regions V3–V4 with the universal bacterial primers 338 F (5′-ACTCCT ACGGGAGGCAGCAG-3′) and 806 R (5′-GGACTACHVGGGTWTCT AAT-3′). The bacterial community was analyzed with an Illumina MiSeq high-throughput sequencing system (Majorbio Bio-Pharm Technology Co., Ltd., Shanghai, China). DNA was separated into fragments with an average size of approximately 300 bp using a Covaris M220 Focused-ultrasonicator (Gene Company Limited, China) for the paired-end library construction with a TruSeq™ DNA Sample Prep Kit (Illumina, San Diego, CA, USA). The adapters containing the full complement of sequencing primer hybridization sites were ligated to the blunt-end fragments. Paired-end sequencing was performed on an Illumina HiSeq4000 platform (Illumina Inc., San Diego, CA, USA) at Majorbio Bio-Pharm Technology Co., Ltd. (Shanghai, China) using the HiSeq 3000/4000 PE Cluster Kit and HiSeq 3000/4000

SBS Kits according to the manufacturer's instructions. Open reading frames (ORFs) from each metagenomics sample were predicted using the MetaGene (http://metagene.cb.k.u-tokyo.ac.jp/). The predicted ORFs with length equal to or greater than 100 bp were retrieved and translated to amino acid sequences using the NCBI translation table (http://www.ncbi.nlm.nih.gov/Taxonomy/taxonomyhome.html/index.cgi?chapter=tgencodes#SG1). All sequences from gene sets with 95% sequence identity were clustered as the non-redundant gene catalog by the CD-HIT (http://www.bioinformatics.org/cd-hit). Reads were mapped to the representative genes with 95% identity after quality control using SOAPaligner (http://soap.genomics.org.cn/), and the gene abundances in each sample were evaluated. BLASTP (Version 2.2.28 + , http://blast.ncbi.nlm.nih.gov/Blast.cgi) was employed for taxonomic annotations by aligning non-redundant gene catalogs against the NCBI NR database with the e-value cutoff of $1e^{-5}$. The KEGG pathway annotation was conducted using BLASTP search (Version 2.2.28 +) against the Kyoto Encyclopedia of Genes and Genomes database (http://www.genome.jp/keeg/) with the e-value cutoff of $1e^{-5}$. Microbial community and metagenomic sequences were submitted to the NCBI and can be retrieved according to the accession number PRJNA874174.

Electrochemical analysis

The electrochemical behaviors of the iron rod were investigated using a three-electrode cell CHI660E electrochemical system (Shanghai Chenhua Co. Ltd., China) at 25 °C. The iron rod, a Pt electrode, and an Ag/AgCl electrode (sat. KCl, 222 mV vs. SHE) were used as the working electrode, counter electrode, and reference electrode, respectively. When the original iron rod was used as the working electrode, it was polished with sandpaper, washed with double distilled water, acetone, and again with double distilled water, and then dried with a paper towel. The counter electrode was degreased with ethanol, washed with sterile deionized water, sterilized with ethanol and washed with sterile deionized water again prior to use. The reference electrode was sterilized with 75% ethanol (Sigma) before use. The 2 mg/L (as N) sodium nitrate solution was bubbled with N_2 for 15 minutes before the electrochemical measurements. Cyclic voltammetry (CV) was conducted at the scan rate of 0.1 mV s^{-1} in the voltage range of +0.9 V to −0.9 V[51]. Electrochemical impedance spectroscopy measurements were performed in the frequency range of 100 kHz to 0.1 Hz at the amplitude of 5 mV[52].

Other analyses

Three replicate water samples were obtained in triplicate experiments conducted under the same conditions but at different times. Water samples were filtered through membranes (0.45 μm pore diameter) and analyzed immediately after collection. The pollutant concentrations in three replicates were averaged for the analysis of pollutant removal performance. The determinations of NO_3^--N, NO_2^--N, and NH_4^+-N were performed according to the standard methods (APHA, 1998). NO_3^--N was determined by Ultraviolet Spectrophotometric Screening Method, NO_2^--N was determined by Colorimetric Method, and NH_4^+-N was determined by Nessler's Reagent-Spectrophotometric Screening Method.

DATA AVAILABILITY

All data are available in the manuscript or the supplementary materials or from the authors on request.

Received: 24 June 2022; Accepted: 20 October 2022;
Published online: 08 November 2022

REFERENCES

1. Reddy, K., Patrick, W. & Broadbent, F. Nitrogen transformations and loss in flooded soils and sediments. *Crit. Rev. Environ. Sci. Technol.* **13**, 273–309 (1984).
2. Ottley, C., Davison, W. & Edmunds, W. Chemical catalysis of nitrate reduction by iron (II). *Geochim. Cosmochim. Acta* **61**, 1819–1828 (1997).
3. Anderson, D. M., Glibert, P. M. & Burkholder, J. M. Harmful algal blooms and eutrophication: Nutrient sources, composition, and consequences. *Estuaries* **25**, 704–726 (2002).
4. Wang, S. et al. Trophic state assessment of global inland waters using a MODIS-derived Forel-Ule index. *Remote Sens. Environ.* **217**, 444–460 (2018).
5. Granger, J., Sigman, D. M., Needoba, J. A. & Harrison, P. J. Coupled nitrogen and oxygen isotope fractionation of nitrate during assimilation by cultures of marine phytoplankton. *Limnol. Oceanogr.* **49**, 1763–1773 (2004).
6. Groffmann, P. M., Zak, D. R., Christensen, S., Mosier, A. & Tiedje, J. M. Early spring nitrogen dynamics in a temperate forest landscape. *Ecology* **74**, 1579–1585 (1993).
7. Burgin, A. J. & Hamilton, S. K. Have we overemphasized the role of denitrification in aquatic ecosystems? A review of nitrate removal pathways. *Front. Ecol. Environ.* **5**, 89–96 (2007).
8. Ward, B. B. How nitrogen is lost. *Science* **341**, 352–353 (2013).
9. Zhang, Y. et al. Dissolved oxygen stratification and response to thermal structure and long-term climate change in a large and deep subtropical reservoir (Lake Qiandaohu, China). *Water Res* **75**, 249–258 (2015).
10. Sun, F. Y. et al. Aerobic methane oxidation coupled to denitrification in a membrane biofilm reactor: Treatment performance and the effect of oxygen ventilation. *Bioresour. Technol.* **145**, 2–9 (2013).
11. Zhang, Q. D., Liu, S., Yang, C., Chen, F. & Lu, S. Bioreactor consisting of pressurized aeration and dissolved air flotation for domestic wastewater treatment. *Sep. Purif. Technol.* **138**, 186–190 (2014).
12. Downing, J. A. et al. Sediment organic carbon burial in agriculturally eutrophic impoundments over the last century. *Glob. Biogeochem. Cycles* **22**, GB1018 (2008).
13. Liang, G. et al. Evaluation of heavy metal mobilization in creek sediment: Influence of RAC values and ambient environmental factors. *Sci. Total Environ.* **607**, 1339–1347 (2017).
14. Schulz, H. et al. Dense populations of a giant sulfur bacterium in Namibian shelf sediments. *Science* **284**, 493–495 (1999).
15. Catling, D. C. & Claire, M. W. How Earth's atmosphere evolved to an oxic state: A status report. *Earth. Planet. Sci. Lett.* **237**, 1–20 (2005).
16. Jelen, B. I., Giovannelli, D. & Falkowski, P. G. The role of microbial electron transfer in the coevolution of the biosphere and geosphere. *Annu. Rev. Microbiol.* **70**, 45–62 (2016).
17. Falkowski, P. G., Fenchel, T. & Delong, E. F. The microbial engines that drive Earth's biogeochemical cycles. *Science* **320**, 1034–1039 (2008).
18. Pfeffer, C. et al. Filamentous bacteria transport electrons over centimetre distances. *Nature* **491**, 218–221 (2012).
19. Nielsen, L. P., Risgaard-Petersen, N., Fossing, H., Christensen, P. B. & Sayama, M. Electric currents couple spatially separated biogeochemical processes in marine sediment. *Nature* **463**, 1071–1074 (2010).
20. Viggi, C. C. et al. Magnetite particles triggering a faster and more robust syntrophic pathway of methanogenic propionate degradation. *Environ. Sci. Technol.* **48**, 7536–7543 (2014).
21. Cord-Ruwisch, R., Lovley, D. R. & Schink, B. Growth of Geobacter sulfurreducens with acetate in syntrophic cooperation with hydrogen-oxidizing anaerobic partners. *Appl. Environ. Microbiol.* **64**, 2232–2236 (1998).
22. Liu, X., Shi, L. & Gu, J. D. Microbial electrocatalysis: Redox mediators responsible for extracellular electron transfer. *Biotechnol. Adv.* **36**, 1815–1827 (2018).
23. Clarke, T. A. et al. Structure of a bacterial cell surface decaheme electron conduit. *Proc. Natl Acad. Sci. U. S. A.* **108**, 9384–9389 (2011).
24. Nakamura, R., Kai, F., Okamoto, A., Newton, G. J. & Hashimoto, K. Self-constructed electrically conductive bacterial networks. *Angew. Chem. Int. Ed. Engl.* **48**, 508–511 (2009).
25. Byrne, J. M. et al. Redox cycling of Fe(II) and Fe(III) in magnetite by Fe-metabolizing bacteria. *Science* **347**, 1473–1476 (2015).
26. Yu, H. & Leadbetter, J. R. Bacterial chemolithoautotrophy via manganese oxidation. *Nature* **583**, 453–458 (2020).
27. Vink, J. P. M. Measurement of heavy metal speciation over redox gradients in natural water-sediment interfaces and implications for uptake by benthic organisms. *Environ. Sci. Technol.* **36**, 5130–5138 (2002).
28. Freguia, S., Tsujimura, S. & Kano, K. Electron transfer pathways in microbial oxygen biocathodes. *Electrochim. Acta* **55**, 813–818 (2010).
29. Fricke, K., Harnisch, F. & Schroeder, U. On the use of cyclic voltammetry for the study of anodic electron transfer in microbial fuel cells. *Energy Environ. Sci.* **1**, 144–147 (2008).
30. Carmona-Martinez, A. A. et al. Cyclic voltammetric analysis of the electron transfer of *Shewanella oneidensis* MR-1 and nanofilament and cytochrome knock-out mutants. *Bioelectrochemistry* **81**, 74–80 (2011).

31. Liang, B. et al. Accelerated reduction of chlorinated nitroaromatic antibiotic chloramphenicol by biocathode. *Environ. Sci. Technol.* **47**, 5353–5361 (2013).
32. Hansen, H. C. B., Borggaard, O. K. & Sorensen, J. Evaluation of the free-energy of formation of Fe(II)-Fe(III) hydroxide-sulfate (green rust) and its reduction of nitrite. *Geochim. Cosmochim. Acta* **58**, 2599–2608 (1994).
33. Weber, K. A., Achenbach, L. A. & Coates, J. D. Microorganisms pumping iron: Anaerobic microbial iron oxidation and reduction. *Nat. Rev. Microbiol.* **4**, 752–764 (2006).
34. Erbs, M., Hansen, H. C. B. & Olsen, C. E. Reductive dechlorination of carbon tetrachloride using iron(II) iron(III) hydroxide sulfate (green rust). *Environ. Sci. Technol.* **33**, 307–311 (1999).
35. Dietl, A. et al. The inner workings of the hydrazine synthase multiprotein complex. *Nature* **527**, 394–397 (2015).
36. Wang, H. B. et al. Effects of microbial redox cycling of iron on cast iron pipe corrosion in drinking water distribution systems. *Water Res* **65**, 362–370 (2014).
37. Chakraborty, A. & Picardal, F. Induction of nitrate-dependent Fe(II) oxidation by Fe(II) in *Dechloromonas sp*. strain UWNR4 and *Acidovorax sp*. strain 2AN. *Appl. Environ. Microbiol.* **79**, 748–752 (2013).
38. Sucheta, A., Ackrell, B. A., Cochran, B. & Armstrong, F. A. Diode-like behaviour of a mitochondrial electron-transport enzyme. *Nature* **356**, 361–362 (1992).
39. Lycus, P. et al. Phenotypic and genotypic richness of denitrifiers revealed by a novel isolation strategy. *ISME J.* **11**, 2219–2232 (2017).
40. Xu, M. Y. et al. Elevated nitrate enriches microbial functional genes for potential bioremediation of complexly contaminated sediments. *ISME J.* **8**, 1932–1944 (2014).
41. Till, B. A., Weathers, L. J. & Alvarez, P. J. J. Fe(0)-supported autotrophic denitrification. *Environ. Sci. Technol.* **32**, 634–639 (1998).
42. Daniels, L., Belay, N., Rajagopal, B. S. & Weimer, P. J. Bacterial methanogenesis and growth from CO_2 with elemental iron as the sole source of electrons. *Science* **237**, 509–511 (1987).
43. Yang, F. et al. Effect of sulfate on the transformation of corrosion scale composition and bacterial community in cast iron water distribution pipes. *Water Res.* **59**, 46–57 (2014).
44. Miot, J. et al. Formation of single domain magnetite by green rust oxidation promoted by microbial anaerobic nitrate-dependent iron oxidation. *Geochim. Cosmochim. Acta* **139**, 327–343 (2014).
45. Myneni, S. C. B., Tokunaga, T. K. & Brown, G. E. Abiotic selenium redox transformations in the presence of Fe(II,III) oxides. *Science* **278**, 1106–1109 (1997).
46. Weber, K. A., Urrutia, M. M., Churchill, P. F., Kukkadapu, R. K. & Roden, E. E. Anaerobic redox cycling of iron by freshwater sediment microorganisms. *Environ. Microbiol.* **8**, 100–113 (2006).
47. Hansen, H. C. B., Koch, C. B., Nancke-Krogh, H., Borggaard, O. K. & Sørensen, J. Abiotic nitrate reduction to ammonium: Key role of green rust. *Environ. Sci. Technol.* **30**, 2053–2056 (1996).
48. Etique, M. et al. Abiotic process for Fe(II) oxidation and green rust mineralization driven by a heterotrophic nitrate reducing bacteria (*Klebsiella mobilis*). *Environ. Sci. Technol.* **48**, 3742–3751 (2014).
49. Wang, H. B., Hu, C., Han, L. C. & Yang, M. Effects of microbial cycling of Fe(II)/Fe(III) and Fe/N on cast iron corrosion in simulated drinking water distribution systems. *Corros. Sci.* **100**, 599–606 (2015).
50. Huang, W. et al. Temperature dependence of spherical electron transfer in a nanosized Fe-14 complex. *Nat. Commun.* **10**, 1–9 (2019).
51. Pocaznoi, D., Erable, B., Delia, M.-L. & Bergel, A. Ultra microelectrodes increase the current density provided by electroactive biofilms by improving their electron transport ability. *Energy Environ. Sci.* **5**, 5287–5296 (2012).
52. Dominguez-Benetton, X., Sevda, S., Vanbroekhoven, K. & Pant, D. The accurate use of impedance analysis for the study of microbial electrochemical systems. *Chem. Soc. Rev.* **41**, 7228–7246 (2012).

ACKNOWLEDGEMENTS

The authors are grateful for financial support from the Fund for Innovative Research Group of NSFC (Grant No. 51721006) and the National Science Fund for Distinguished Young Scholars (Grant No. 21925801).

AUTHOR CONTRIBUTIONS

All authors contributed intellectual input and assistance to this study. H.Z.Z. and Q.Z.Y. conceived the initial idea and experimental design. M.E. and H.Z.Z. supervised the study and experiments; M.Z.W., J.W.L. and A.X. performed the research; M.Z.W., J.W.L., H.W., A.X., J.R.N. and L.R.W. analyzed the data and M.Z.W., J.W.L., L.R.W., M.E. and H.Z.Z. wrote the paper. All author contributed to the final version of the manuscript. M.Z.W. and J.W.L. contributed equally to this work.

COMPETING INTERESTS

The authors declare no competing interests.

ADDITIONAL INFORMATION

Supplementary information The online version contains supplementary material available at https://doi.org/10.1038/s41545-022-00205-x.

Correspondence and requests for materials should be addressed to Menachem Elimelech or Hua-Zhang Zhao.

Reprints and permission information is available at http://www.nature.com/reprints

Publisher's note Springer Nature remains neutral with regard to jurisdictional claims in published maps and institutional affiliations.